HHS Public Access

Author manuscript

Nanotoxicology. Author manuscript; available in PMC 2016 March 08.

Published in final edited form as:

Nanotoxicology. 2015 ; 9(7): 871–885. doi:10.3109/17435390.2014.986670.

Implications of in-vitro dosimetry on toxicological ranking of low aspect ratio engineered nanomaterials

Anoop K. Pal[1,3], **Dhimiter Bello**[2,3,*], **Joel Cohen**[3], and **Philip Demokritou**[3,*]

[1]University of Massachusetts Biomedical Engineering and Biotechnology Program, MA 01854, USA

[2]Department of Work Environment, College of Health Sciences; University of Massachusetts Lowell, Lowell, MA 01854, USA

[3]Center for Nanotechnology and Nanotoxicology, Department of Environmental Health, Harvard School of Public Health, 677 Huntington Avenue, Boston, MA 02115, USA

Abstract

In-vitro high throughput screening platforms based on mechanistic injury pathways are been used for hazard assessment of engineered nanomaterials (ENM). Toxicity screening and other *in vitro* nanotoxicology assessment efforts in essence compare and rank nanomaterials relative to each other. We hypothesize that this ranking of ENM is susceptible to dispersion and dosimetry protocols, which continue to be poorly standardized. Our objective was to quantitate the impact of dosimetry on toxicity ranking of ENM. A set of eight well-characterized and diverse low aspect ratio ENMs, were utilized. The recently developed at Harvard *in-vitro* dosimetry platform, which includes preparation of fairly monodispersed suspensions, measurement of the effective density of formed agglomerates in culture media and fate and transport modeling was used for calculating the effective dose delivered to cells as a function of time. Changes in the dose-response relationships between the administered and delivered dose were investigated with two representative endpoints, cell viability and IL-8 production, in the human monocytic THP-1 cells. The slopes of administered/delivered dose-response relationships changed 1:4.94 times and were ENM-dependent. The overall relative ranking of ENM intrinsic toxicity also changed considerably, matching notably better the *in vivo* inflammation data (R^2 0.97 vs. 0.64). This standardized dispersion and dosimetry methodology presented here is generalizable to low aspect ratio ENMs. Our findings further reinforce the need to reanalyze and reinterpret in-vitro ENM hazard ranking data published in the nanotoxicology literature in the light of dispersion and dosimetry considerations (or lack thereof) and to adopt these protocols in future in vitro nanotoxicology testing.

[*]Corresponding authors: Prof. Dhimiter Bello, Associate Professor, Department of Work Environment; University of Massachusetts Lowell; One University Ave; Lowell, MA 01854, USA, Dhimiter_Bello@uml.edu, Tel: 978-934-3343. Prof. Philip Demokritou, Associate Professor, Department of Environmental Health, Harvard School of Public Health, 677 Huntington Avenue, Boston, MA 02115, USA, pdemokri@hsph.harvard.edu, Tel: 617-432-3481.

Competing Interest The authors declare they have no competing financial interest.

Keywords

in vitro nanotoxicology; effective density; effective dose; dispersion; dosimetry

INTRODUCTION

Rapid development and commercialization of nanotechnology has produced an overwhelmingly large number of engineered nanomaterials (ENMs). Variation in physicochemical properties such as size, surface modifications, crystalline phase, and impurity content for each ENM, results in hundreds of additional materials (Ayres et al., 2008). More scenarios along the life cycle of nano-enabled products further result in exposures to incidental nanomaterials whose properties may be significantly altered compared to the initial raw materials. To match the pace of ENM synthesis and development with toxicity assessment, high throughput approaches based on mechanistic injury pathways have been proposed for ENM screening (Nel et al., 2013b, Jan et al., 2008, Watson, 2014, E.H. Zhou, 2014). *In-vitro* cell based systems (single cell line or co-cultures) are the most common *in vitro* testing platform; their widespread use being driven by lower costs and simpler systems as compared to *in-vivo* testing. Toxicological outcomes from *in vitro* systems are being used for initial screening and ranking of ENMs, as well as to investigate influence of various physicochemical parameters (such as size, shape and surface activity) on ENM toxicity (Luyts et al., 2013, Jones and Grainger, 2009, Warheit et al., 2007).

For *in-vitro* testing, ENMs, which are normally agglomerated in nanopowder form, have to be dispersed in certain liquid medium and eventually transferred into a physiologically relevant media, typically cell culture growth media. The size, size distribution, and the overall dispersion stability (re-agglomeration rate) are dependent on the dispersion protocols (i.e. dispersion conditions and dispersant utilized). These dispersions, when applied for cellular testing, can lead to re-agglomeration and formation of agglomerates larger than the primary particle size of ENMs. More importantly, the effective density of these agglomerates differs from the density of the raw material, at times by several folds, primarily because of the protein corona formation and intra-particle trapping of culture media (DeLoid et al., 2014). The effective density and agglomeration size influence the fate and transport of ENMs in cell media, and defines their settling rate, as well as the other dose metrics such as delivered mass, surface and particle number (DeLoid et al., 2014, Cohen et al., 2013, Cohen et al., 2014a). Furthermore, effective density and agglomeration potential of ENMs *in-vitro* may also alter the dissolution rate and available surface for bio-interactions. The formed agglomerates of nanoparticles *in-vitro* have been shown to exert different biological effects as compared to well-dispersed nanoparticles (Buford et al., 2007, Sharma et al., 2014, Sager et al., 2007). To this effect, several studies have focused on developing dispersion protocols that result in stable nanoparticle dispersion in physiologically relevant *in-vitro* conditions (Cohen et al., 2013).

It is worth noting that, despite its great importance in an *in-vitro* system, effective density it rarely measured as part of the characterization of ENM liquid suspensions. Methodologically, effective density is also difficult to measure because it requires laborious

experiments and expensive instrumentation, such as Analytical Ultracentrifugation Centrifuges (AUC), which is not commonly available in nanotoxicology labs. Recently, a fast and simple method called Volumetric Centrifugation Method (VCM) has been developed at Harvard that enables nanotoxicologists to measure effective density of ENMs in suspension (DeLoid et al., 2014).

A second critical consideration, besides dispersion quality, is the need to assess the dose delivered to cells, which may be quite different from the administered doses usually reported in *in-vitro* studies. *In vitro* nanotoxicology is often comparative in nature because it involves the use of positive or negative ENM materials. The impact of inadequate characterization of dispersion and dosimetry often goes unaccounted for, and may contribute to irreproducible results within- and especially between-laboratories, skewed relationships between toxicological outcomes and physicochemical properties, conflicting findings, and possibly even wrong conclusions when materials get compared with each-other. Evidence documenting these effects are slowly emerging (Hinderliter et al., 2010, Demokritou, 2012, Sharma et al., 2014, Limbach et al., 2005, Teeguarden et al., 2007, Summers et al., 2011). For these reasons, development of an integrated, standardized, reproducible, and generalizable dispersion and dosing approach for toxicity evaluation of ENM(s) remains a priority in *in vitro* nanotoxicology. Important early contributions in developing standardized dispersion protocols (Buford et al., 2007, Bihari et al., 2008, Sager et al., 2007, Vippola et al., 2009, Cohen et al., 2013) delivered dose models (Cohen et al., 2013, Hinderliter et al., 2010, Teeguarden et al., 2007) and dose metric (Warheit et al., 2007) have laid the ground work for a more generalizable approach.

A simple to use, standardized, and integrated platform across the dispersion-dosimetry continuum referred as Harvard Dispersion Dosimetry Platform (HDDP) was developed by the authors and used to estimate dosimetry *in-vitro*. This two step integrated dosimetry approach is based upon the preparation of a well dispersed suspension of ENMs, measurement of the effective density and size of formed agglomerates using the VCM method and the use of advanced numerical models to derive the delivered to cell dose metrics (DeLoid et al., 2014, Cohen et al., 2014a, Cohen et al., 2014b). Furthermore, simple mathematical functions for a given media-ENM system called relative *in-vitro* dose functions (RID), were derived from curve fitting of the numerical model output as described in detail in the Cohen et al., 2014b paper. The RID functions may be used to calculate the settling rate of formed agglomerates as well as their mass, surface and number dose metrics as a function of time for the specific ENM type, cell culture medium, well plate combination so are(DeLoid et al., 2014, Cohen et al., 2013, Cohen et al., 2014b). The RID functions are provided in Table 2 in addition to the VCM-ISDD model estimates not as a substitute for them. While we encourage the use of VCM-ISDD and other more sophisticated numerical models for dose estimation, we believe that in their absence, and provided that the *in vitro* system is identical or very close to the conditions that for which RID functions were derived (as described in Table 2), the delivered dose estimates based on RID functions do provide a good approximations and significant improvement over not considering dosimetry at all.

Here in this companion study, the aforementioned HDDP hybrid dosimetric methodology as described in great detail by the authors in their two recent publications (Cohen et al., 2014b,

Deloid et al, 2014) has been utilized to investigate the link between dosimetry and *in-vitro* toxicological outcomes for low aspect ratio ENMs, including carbon based ENMs and metal alloys. More importantly, the effect of dosimetry on *in-vitro* toxicological ranking of ENMs was assessed. Eight ENM from different classes and covering a wide range of physicochemical properties (size, shape, material density) were selected. These ENMs were dispersed using the previously developed standardized dispersion protocol in a physiologically relevant cell culture medium, followed by in-liquid media characterization, which included measurement of the effective density of the formed agglomerates, using the Harvard VCM method. THP-1 cells were dosed over a range of ENM concentrations (5 points, 1–50 μg/mL administered dose). The delivered dose to cells was calculated using the previously reported dosimetry method (Cohen et al., 2013, DeLoid et al., 2014). The impact of dosimetry considerations using this standardized dispersion-dosimetry platform was assessed *in-vitro* in THP-1 cells using cell viability and cytokine release as representative endpoints. It was demonstrated here that the proposed approach is generalizable for low aspect ratio ENMs and essential for meaningful *in vitro* comparative toxicity assessment.

MATERIALS and METHODS

Nanomaterial characterization in nanopowder form

Eight ENM investigated in this study and summarized in Table 1 included: carbon black (N110) (Bello et al., 2009, Hsieh et al., 2013), Printex-90 (Elder et al., 2005, Sager and Castranova, 2009), H_2O_2 oxidized single wall carbon nanohorns (SWCNHs-ox) (Bello et al., 2009, Hsieh et al., 2013), titanium dioxide (TiO_2 P25) (VanWinkle et al., 2009, Keller et al., 2010), cerium oxide (CeO_2) (Keller et al., 2010), manganese oxide (MnOx PALAS) (VanWinkle et al., 2009), silver (VanWinkle et al., 2009, Rushton et al., 2010), and Nickel nanoparticle (NI-Inco) developed for catalytic applications (Inconel). These materials have been extensively characterized in the dry-state and reported in previous studies, as summarized in Table 1. Briefly, characterization of dry powders included transmission electron microscopy for primary size and morphology, specific surface area by BET, X-ray diffraction for crystallinity, total and water-soluble metals by inductively coupled plasma mass spectrometry (ICP-MS), and organic and elemental carbon. In addition, all materials were characterized for their ability to induce biological oxidative damage using a serum based Ferric Reducing Ability of Serum Assay (FRAS), as reported elsewhere by us (Hsieh et al., 2013).

Engineered nanomaterial dispersion and characterization

The protocol developed recently by Cohen et al., (2013) and illustrated schematically in Figure 1 was used for ENM dispersion. Briefly, all ENMs were sonicated at the predetermined critical sonication energy (DSE_{cr}) and ENM stock solutions (5 mg/mL) were further diluted to 0.5 mg/mL in RPMI + 10% FBS, followed by a mixing step for 2 h on a multi-stirrer plate. This mixing step improves stability and size of dispersion for certain difficult-to-disperse ENM, such as Ni-Inco, as shown in the supplemental information. As a standard practice, we do purge the dispersion medium with nitrogen, in order to minimize dissolved oxygen and subsequent oxidation of metal ENM (e.g. Ag). Z-Average Hydrodynamic diameter $d_{(h,\ z\text{-}ave)}$, polydispersity index (PdI) and zeta potential (ζ) for

ENM dispersions were determined by dynamic light scattering (DLS) using a Malvern Zetasizer Nano-ZS instrument. Confirmation of DLS measurements with a secondary technique is desirable (Warheit et al., 2007). Particle morphology and size of ENMs in the RPMI+10% FBS dispersions were further characterized using transmission electron microscopy on a Philips EM 400T. In addition to using TEM, we also used a new high-resolution tunable resistive pulse sensing technology (TRPS, qNano from Izon Scientific, Boston, MA) to verify size distribution (Pal et al., 2014). TRPS measures changes in electrical conductivity as the nanoparticles pass one-by-one through a nanopore (Roberts et al., 2010, Willmott et al., 2010). TRPS employs a fundamentally different measurement principle compared to DLS, and it is an independent confirmation technique (Anderson et al., 2013). Detailed descriptions of dispersion and characterization techniques are presented in the supplementary section.

Determination of effective density

Effective density of all ENM samples was determined by using the recently developed Harvard VCM method (Cohen et al., 2014b, DeLoid et al., 2014). Briefly, 50 μg/mL ENM suspensions was aliquot into TPP packed cell volume (PCV) tubes (Techno Plastic Products, Trasadingen, Switzerland) and centrifuged at 1,000× g for one hour. Agglomerate pellet volume, was measured using a slide rule-like easy-measure device also obtained from the PCV tube manufacturer. Effective agglomerate density was calculated from agglomerate pellet volume values of each ENM and condition as described in (Demokritou, 2012, Cohen et al., 2014b, DeLoid et al., 2014). Delivered dose values were calculated based on inputs of DLS-measured agglomerate diameter and VCM measured effective density using the VCM-ISDD model, as described in detail in Cohen et al., 2014b

RID functions

The Relative in Vitro Dose (RID) functions, which calculate deposited fraction of mass, surface area and particle number concentration as a function of exposure time, for all ENMs in this specific cell culture system (media type, well parameters, etc.) were derived as detailed in (Cohen et al., 2014b). The deposition fraction constant, α (h^{-1}), needed for the RID functions, was derived from curve fitting of the VCM-ISDD numerical model output. Furthermore, the time required for the delivery of 50% and 90% of the administered dose, t50 and t90 respectively, was calculated for each ENM as described in the aforementioned references. The RID functions are not used in dosimetry calculations in this paper; they have been provided here for reference and as part of the overall platform.

Cell culture and ENM dosing

Human monocyte/macrophage (THP-1) leukemia cell line was used in this study. Cells were grown and maintained in RPMI 1640 medium containing 10% heat-inactivated FBS and supplemented with penicillin G 50 U/mL and streptomycin sulfate 50 μg/mL, in 75 cm^2 cell culture flasks (Corning) at 37°C in 5% CO_2 humidified incubator. When confluent, THP-1 cells were centrifuged and seeded in 96-well plates (VWR) at 5×10^5 cells/mL (total volume 200 μL/well), in the presence of 20 ng/mL phorbol myristate acetate (PMA, Sigma-Aldrich,) in order to differentiate them into mature macrophage- like cells (for MTT and cytokine release experiments). Twenty-four hours after seeding, 100 μL of the medium was

removed and cells were treated with different ENM mass concentrations (0, 1, 5, 10, 30 and 50μg/mL) or an equivalent amount of medium alone, and the final volume was adjusted with media to 200 μL. All experiments were performed in triplicates. RPMI+10% FBS and PBS were used as negative control for each time point in all the treatment cell culture plates. Supernatants collected from cells induced with LPS (1 μg/mL final concentration) were used as reference positive control for cytokine analysis. All nanoparticles were treated with Polymyxin B to neutralize any endotoxin contamination.

MTT assay cellular viability

Cell viability was evaluated with the MTT assay kit (ATCC) based on reduction of the yellow tetrazolium salt MTT (3-(4,5 dimethylthiazol-2-yl)-2,5-diphenyltetrazoliumbromide) to a purple, insoluble MTT-formazan. Cells were maintained in RPMI+10% FBS and plated in 96 wells plate as described above and exposed to ENM dispersions for 24 h. Afterwards, the cells were washed twice with 100 μL of PBS and incubated with MTT reagent in 200 μL RPMI+10% FBS for 3–4h. Afterwards, the medium was removed and replaced by 200uL of detergent to dissolve the MTT-formazan crystals. The plates were then kept for 5–6 h in the incubator followed by light absorption measurements. The readings were measured at 550 nm (reference wavelength at 670 nm) in a spectrophotometer (BioTek Synergy, VT). Triton X-100 (0.01%) was used as positive control, whereas medium alone was used as a negative control.

Cytokine analysis

The media supernatants were harvested after 24 h of treatment and stored at −80°C TM degree, which were later used to perform cytokine analyses using Luminex (x-Map) technology). Samples were assayed using a 13-plex high sensitivity human cytokine Kit (Millipore, Billerica, MA) according to the manufacturer's instructions. The results were analyzed using a Luminex 200IS System (Luminex Corporation, Austin, TX). Cytokine concentrations were calculated using Upstate Beadview (Temecula, CA) software. Here, IL-8 is used as a representative cytokine for comparative purposes.

Microscopy

For microscopy analysis, 5×10^4 THP-1 cells were seeded in 1 mL of culture medium in 12-well plates and were grown and allowed to attach for 24 h on glass coverslips in the wells as described above. Cells were treated with 50 μg/mL ENM suspension for 24h. The ENM medium was then removed and cells were washed twice with PBS. Cells were then fixed with 4% paraformaldehyde and coverslips were mounted on a glass slide for microscopy. The image data were taken using a Zeiss 710 laser scanning confocal instrument.

Toxicity response assessment

The initial toxicity assessment for all ENMs for these representative endpoints was done on the basis of administered doses (μg/ml) to the cells. A complete dose range toxicity assessment was conducted to determine Inhibitory Concentration (IC) mass dose for all nanomaterials with cell viability as toxicity endpoint. As discussed earlier, further dose calculations for all ENMs were done to convert the administered doses to delivered mass

doses (μg). Further, the IC25 mass values for each ENM was used to extrapolate IL-8 cytokine release at that delivered mass and comparisons were made with the slopes of dose-response curves for each dose. It should be noted that alternative metrics based on number concentration (directly measured by TRPS and calculated by the dosimetry model) and mass per unit surface area of cells are available and will be used in subsequent multiparametric analysis of multiple toxicity endpoints and PCM properties. Because several of these dose metrics are highly correlated with each-other (e.g. deposited mass in pg/cell and deposited number concentration in number particles/cell), the outcome of the comparative analysis based on the mass matric remains unchanged.

In vivo to in vitro comparisons

In vivo lung inflammation data (polymorphonuclear leukocytes (PMN) cells in the bronchoalveolar lavage of rodents) after 24 h of intra tracheal ENM instillation for a subset of five out of eight ENM was obtained from the published literature as referenced in Table 1 and 5 as follows: Printex-90 and nano TiO_2 from (Sager and Castranova, 2009, Baisch et al., 2014), and ceria from (Ma et al., 2011). For Ni Inco and nAg, the PMN data was kindly provided by Prof. A. Elder, University of Rochester, USA. The *in vivo* lung inflammation data were normalized to PMN cells/μg instilled ENM. No suitable data were found for three materials: SWCNH-ox, N110, and MnOx. The *in vivo* PMN data was compared to cell viability slopes (% dead cells/μg ENM) in regression analysis.

Statistical analysis

Statistical differences between groups were tested via repeated measures two-way ANOVA, Tukey multiple comparison test, in Graphpad prism software 5 Inc, CA, USA. Regression analysis and Spearman rank order was used to compare in vitro data to in vivo lung inflammation. All experiments were repeated three independent times (n = 3). Results were considered statistically significant at $p < 0.05$. Results are expressed as mean ± SD or otherwise stated.

RESULTS

Particle characterization of dry ENM powder

The selected set of low aspect ratio ENM covered a broad range of ENM physicochemical properties (sizes, shapes, surface area, metal content, surface chemistry and material densities). Key physicochemical properties of the dry powders, most relevant to the current investigation, are summarized in Table 1. SSA for carbon based ENMs ranged from 111 m^2/g for N110 to as high as 1154 m^2/g for SWCNH-ox, whereas for metal/metal oxide group, SSA varied from 18 m^2/g for nAg to a maximum of 91 m^2/g for Ni Inco. The material powder density of ENMs varied considerably for metal/metal oxides ENMs (range of 4.25–10.50g/cm^3) in comparison to that of carbon based ENMs (range 1.25–1.85 g/cm^3). The primary particle size by BET and XRD compared reasonably well. Interested reader can find additional characterization for these materials in the referenced publications.

Bio-relevant ENM dispersion and its stability

As depicted in Figure 1 and described in methods, a previously published (Cohen et al., 2013) dispersion protocol was used. Figure 2 shows the effect of increasing sonication energy on ENM hydrodynamic size $d_{(h, z\text{-}ave)}$ in DI water as measured by DLS. A familiar asymptotic curve was observed for $d_{(h, z\text{-}ave)}$ as a function of sonication energy for SWCNH-ox, TiO_2 P25 and nAg (Figure 2). For ENMs like Ni-Inco and MnOx-PALAS a U-shaped pattern was observed (Figure 2), highlighting the fact that sample over sonication can result in higher sizes for nanomaterials and that experimental determination of DSE_{cr} is important. To the best of our knowledge, this is the first time such a U-shaped curve has been reported. For the majority of ENMs, DSE_{cr} was close to 262 J/mL except for SWCNHs-ox and TiO_2 P25 with DSE_{cr} at 161 J/mL. Table 2 further summarizes the DLS measured ENM properties (size, PdI and zeta potential) for all the ENMs in DI water at DSE_{cr} sonication energy. Except for Ni-Inco (1791.3 ± 51.7 nm) and MnOx-PALAS (1489.5 ± 44.5nm), the $d_{(h, z\text{-}ave)}$ obtained for all ENMs were in the nano size range. These two materials were chosen because they were known to us to be difficult to disperse. For CeO_2 and nAg, the sizes measured were close to 100nm, whereas for TiO_2 P25 the $d_{(h, z\text{-}ave)}$ was 336.0 ± 9.0 nm. The polydispersity values were in the range of 0.20 to 0.61 depending on ENM type. The difference in sizes and polydispersity correlated well with Zeta measurements as the dispersion with zeta values higher than −30mV and +30mV are considered stable (Vippola et al., 2009). With the exception of SWCNH-ox, N110 and nAg, all other ENMs had positive zeta potential values (charges) in DI water. As expected, Ni-Inco and MnOx PALAS had very low zeta values owing to fast sample aggregation and coarse agglomerates formation, consistent with previous reports by the authors (Cohen et al., 2013).

For these difficult to disperse ENM, addition of a mixing step in the dispersion protocol improved significantly the size and stability of certain metal oxides ENM dispersions, as can be seen especially for MnOx PALAS and Ni-Inco (supplemental information, Table S1). Optimization experiments on the effects of mixing, duration, and concentration of FBS (0–10%) used for stabilizing ENM dispersions suggested that mixing had a notable effect during the first 2 h and it is a necessary step for certain ENM. Stable ENM dispersions could be achieved only with at least 10% FBS. The effect of mixing duration, % of FBS used for stabilizing ENM suspensions (Figure S1, S2 and Table S1), had a considerable effect on the deposited ENM doses, as observed through optical microscopy images (Figure S3), and also translated to differences in toxicity patterns as seen with cell viability (Figure S4). As expected, unstandardized and suboptimal dispersion protocols lead to significant variations in outcomes and irreproducible results, and robust standardized dispersion protocols should be used. Here we focus only on the impact of using an integrated dispersion and dosimetry platform on toxicity ranking of different ENM.

Table 2 further details charge of all ENMs dispersed in RPMI+10% FBS condition after 24h mixing. It also highlights the consistent stability of all ENMs over a period of 24h. All the dispersions had a zeta potential closer to −12mV, typical of RPMI+10% FBS medium. ENMs with positive zeta values in DI water (Ni-Inco, CeO_2 and Printex-90) had much higher polydispersity, agglomeration and aggregation as compared to ENMs with negative

zeta values in DI water (SWCNH-ox and N110). The size and morphology of all ENMs dispersions (in RPMI+10% FBS) was further characterized using Transmission Electron Microscopy (TEM) and the data is summarized in the insert images in Figure 3, alongside DLS size distributions. TEM is a commonly used confirmatory technique for such purposes. It should be reminded though that sample preparation (transfer onto the TEM grid and drying) and TEM imaging conditions (high vacuum and high energy beam) may and often do induce changes in the agglomerate size and morphology and these observations should be interpreted as indicative rather than confirmatory. Keeping this in mind, Figure 3 inserts show that SWCNHs-ox and nAg had spherical geometry in contrast to more variable morphologies observed for N110, Printex-90, TiO_2, Ni-Inco and MnOx PALAS. CeO_2 nanoparticle in dispersion preserved the cubical morphology typically seen in dry state. TEM images for Ni-Inco and MnOx PALAS also confirm the higher polydispersity of these ENMs. Overall, TEM imaging agrees well qualitatively with the DLS measurements.

Dosimetry

Table 3 reports the VCM measured effective densities of all ENMs. For carbon based ENMs, the effective densities (1.04–1.25 g/cm^3) were only slightly different from their respective raw material densities (1.25–1.85 g/cm^3). In contrast, the effective densities of metal/metal oxide ENMs (1.31–2.30 g/cm^3) were significantly smaller in comparison to their raw material densities (4.25–10.50 g/cm^3). Particle effective density and particle size in dispersion medium (i.e. material agglomeration state) plays an important role in determining particle mobility in suspension and thus the overall ENM dose delivered to the cells *in-vitro* (Cohen et al., 2013, Cohen et al., 2014b, DeLoid et al., 2014).

In addition, Table 3 summarizes the administered dose, particle- and media-specific deposition fraction constant, α (h^{-1}), VCM-ISDD estimated deposited doses and time required to deliver 90% of the administered dose to cell, t_{90} (h) for all ENMs dispersed in RPMI+10% FBS condition. Figure 4 illustrates the VCM-ISDD derived time elapsed estimated deposited dose for all ENMs, as described in detail in Cohen et al 2014b.

Effective density influences deposition fraction constant, α and t_{90}. ENMs with higher effective density value aggregates (mostly metal/metal oxides) had a comparatively larger α values and lower t_{90} values in contrast to ENMs with lower effective density value aggregates (carbon based ENMs). Consequently, SWCNH-ox, and N110 had t_{90} values higher than 200h whereas ENMs like TiO_2, CeO_2 and nAg had t_{90} values less than 50h indicating high dose deposition, as illustrated by the deposition fraction curves in Figure 4. Note that ~5–30% of the administered dose was delivered to cells at 6h, with greater differences in the delivered dose observed at 24 h (~15% for SWCNH-ox and N100 to ~95% for TiO_2 P25).

For this study, currently available mathematical models for calculating deposited dose were utilized, that do not account for dynamic changes to agglomerate characteristics over time that can occur in various physiological media. As shown in Table 2, slight changes to agglomerate diameter may occur over the course of an *in vitro* exposure, and these slight shifts may impact the delivered to cell dose over time. Currently our group is working to develop more sophisticated models that account for dynamic changes to particle size and

density over time that will more accurately reflect these changes and their impact on dosimetry. Moreover, agglomerate stability over time is greatly affected by dispersion protocol, re-emphasizing the importance of standardized and optimized protocol to ensure agglomerate properties remain as stable as possible throughout the duration of an *in-vitro* assay.

Confirmation of dispersion measurements by TRPS

The size distributions of dispersions measured by TRPS are summarized in Table 4. The typical size distributions as measured by DLS and TRPS are illustrated for SWCHN-ox in Figure 5. The TRPS distribution was typically bimodal, with a secondary peak of a subpopulation of larger agglomerates, consistent with TEM image analysis. The DLS gave a single much broader peak. This skewing in the distribution is expected for DLS and is a result of higher intensity light scattering by the larger agglomerates. For the purpose of this study, we decided to use only DLS size distribution data. It has to be acknowledged that both DLS and TRPS measure size and size distributions through different principals and that comparison of measurements from these two techniques should be interpreted with caution.

Cellular toxicity

Two endpoints of cellular toxicity, namely mitochondrial activity via the MTT assay and IL-8 cytokine release (a pro-inflammatory marker), were assessed in THP-1 cells for all ENM dispersions in RPMI+10% FBS at 24h exposure at doses ranging from 1μg/mL to 50μg/mL ENM. We emphasize that the main purpose of cytotoxic evaluations here was to investigate the effect of ENM dose deposition kinetics on these representative cellular responses and assess the magnitude of impact dosimetry has in the relative comparison of these materials. In-depth analysis of a comprehensive set of cytotoxicity endpoints (such as mRNA expression of several genes, intracellular oxidative stress, and multiple cytokine/chemokine production) at different time points will be subject of subsequent manuscripts. Figure 6 (black symbols and fitted lines) shows the cell viability results for all ENMs dispersed in RPMI+10% FBS for 24h incubation as a function of administered (black) and delivered (red) dose. Cell viability decreased linearly with the administered mass dose but at different slopes. SWCHN-ox, Ni-Inco, MnOx PALAS and nAg showed higher cellular death rates per unit mass, causing ~ 55–60% cell death at the highest dose of 50μg/mL. TiO_2-P25 and CeO_2 did not induce significant cell death, whereas N110 and Printex-90 induced 30% cell death at 50μg/mL. For carbon based materials, notable differences were observed in the slopes of delivered doses compared to the administered doses. SWCNH-ox and N110 were seen to have a deposited dose approximately 20% of the administered dose (~5x steeper slope for delivered dose), whereas for Printex-90 it was 34% (slope ratios of ~3x). For metal and metal oxide ENMs, the deposited fractions were much higher than for carbonaceous ENM, ranging from 44.6% for Ni-Inco to 98.4% for TiO_2-P25, resulting in smaller differences between the administered and delivered dose slopes.

These differences, under normal circumstances, without dosimetry corrections, would go unnoticed and can affect the final toxicity analysis and relative ranking order. The Inhibitory concentration (IC25) values, i.e. mass dose at which 75% cells will be live, were derived from the fitted linear regression lines on the dose-response curves. Table 5 summarizes the

slopes for cell viability plots as well as IC25 values for all ENMs based on administered and deposited doses. ENMs like SWCNH-ox with low deposited dose rates and low cell viability had a very steep negative slope and consequentially much smaller IC25 values (0.58 μg), as compared to ENMs like TiO_2 P25 and CeO_2, with high deposition rates and higher cell viability and IC25 greater than 10μg.

Figure 7 shows IL-8 cytokine release as a function of administered and deposited dose for all ENMs dispersed in RPMI+10% FBS at 24 h. The IL-8 cytokine release values for all ENMs at most of the tested concentrations were significantly higher (t-test, $p < 0.05$) than that of PBS control except for lower doses of N110, TiO_2 and Printex-90. The slopes of IL-8 release as a function of administered or deposited mass doses varied drastically. Carbon based ENMs had highest slope changes followed by MnOx PALAS and Ni-Inco. With minor exceptions, the relationship of IL-8 production with ENM dose follows a sigmoidal curve; at the highest administered dose of 50μg ENM/mL, the IL-8 production is much higher than the predicted trend from the first three ENM doses. For Printex-90 and nAg, the IL-8 concentrations at the highest 50 μg/mL dose were above the upper detection limit of the instrument. As reported in the literature, it is possible that the high production rate and much higher variability in IL-8 concentrations may be a result of competing factors: either interaction of ENM with IL-8 and/or due to high ENM cell toxicity. PBS (3.72 ± 0.34 ng/ml IL-8 release) was used as a negative control and LPS (16.0 ± 0.5 ng/mL IL-8 release) as a positive control. The lower limit of detection for IL-8 was 2 pg/mL, whereas the upper limit of quantitation 50 ng/mL. All fitted sigmoidal curves had a R^2 of 0.95 or better. The slopes of the steepest region of the fitted sigmoidal curves were determined by the Origin software and are used for further analysis as summarized in Table 5.

Figure S5 shows Bright-field images of THP-1 cells after dosing with ENMs dispersed in RPMI+10% FBS with 50μg/ml mass concentration for 24h. The control image (without ENM dosing) shows THP-1 cells without any morphological changes. For s dosed with ENMs, cellular uptake can be seen for all nanomaterials. ENMs either in the cells or on the cell surface were observed as dark spots in the microscopic images. Larger particle agglomerates engulfed/attached to the cells were seen for carbon based ENMs compared to nAg, Ni-Inco and MnOx-PALAS NMs. High ENM deposition was also observed for TiO_2 and CeO_2.

In vitro to in vivo comparison

Figure 8 plots PMN (cells/μg ENM) against cell viability slopes (% dead cell/μg ENM) for both administered and delivered cell doses. Note that correction for delivered dose to cells has a notable impact on the strength of association between *in vivo* inflammation and *in vitro* cell viability (or death) as the R^2 increased from 0.64 to 0.97. Although the dataset is limited to five ENM, it still shows convincingly the utility of the approach presented here and the benefit of estimating delivered dose to cells. A larger dataset, which includes the remaining three materials, should be used for more robust validation of *in vitro* data to *in vivo* results, and is subject of a subsequent manuscript. It is important to note here that the PMA induced THP-1 cell line used in this study is a reasonably good *in vitro* system for predicting *in vivo* lung inflammation and is consistent with the qualitative comparison in Khatri et al., (2013)

and Pirela et al., (2013) whereby PMA induced THP-1 cells matched better *in vivo* inflammation in humans and rodents than human primary nasal and small airway epithelial cell lines.

DISCUSSION

ENM dispersion for in vitro nanotoxicology

The National Academy of Sciences report on 'Toxicity Testing in the 21st Century: A Vision and a Strategy", advocates in favor of high-throughput approaches that utilize mechanistic, and pathway-based toxicity testing in human cells or cell lines with validation in whole organisms (Krewski et al., 2010). These *in vitro* high throughput screening approaches for engineered nanomaterials are currently being developed in leading research centers (Nel et al., 2013b, Nel et al., 2013a, Thomas et al., 2011, Jan et al., 2008). Of all steps involved in these *in vitro* testing, dispersion and cellular dosimetry at realistic/reasonable doses of nanomaterials are critical for effective *in-vitro* testing, and if not done accurately can lead to conflicting and even invalid results (Powers et al., 2006). Development of an integrated dosimetry platform which includes standardized, reproducible, and generalizable dispersion protocols across ENMs with diverse physicochemical properties, followed by determination of effective doses delivered to cells, are critical requirements for meaningful cross comparisons and relative toxicity assessment of nanomaterials and for *in-vivo* validation studies (Cohen et al., 2013, Ahmad Khanbeigi et al., 2012, Cohen et al., 2014b).

In this study we utilized the integrated HDDP methodology recently developed at the Harvard Center for Nanotechnology and Nanotoxicology, which includes the sequence of suspension preparation steps, effective density measurements of ENM agglomerates in cell culture media, and numerical estimation of delivered dose to cells (Cohen et al., 2014b). We investigated the generalizability of this *in vitro* dosimetry platform for a variety of low aspect ratio ENMs including C-based, metals, metal oxides, and metal alloys. The more challenging C-based ENM and metal alloys have been tested for the first time using this integrated dosimetry approach and their RID dosimetry functions were derived. The impact of dose differences (administered vs. delivered) on cellular toxicity outcomes and rank order of this set of ENM was assessed in THP-1 cells using the slopes of dose-response for two endpoints, cell viability and inflammatory cytokine IL-8 production. Furthermore, the *in vitro* cellular responses were compared favorably to *in vivo* PMN data for a subset of five ENM.

Cellular Dosimetry: Delivered vs. administered dose

Recent studies have shown that ENM dispersion status has a profound effects on the effective dose that cells receives, owing to difference in particle–particle and particle to physiologic fluid interactions in the liquid test suspension. Dose for nanoparticles in an *in vitro* system is more dynamic, more complicated, and less comparable across particle types than it is for soluble chemicals. Particles settle, diffuse and agglomerate at rates that differ in relation to their size, effective density, and surface physiochemistry (Hinderliter et al., 2010, Teeguarden et al., 2007).

Real-time techniques to directly assess effective dose delivered to cells from suspensions are limited and material specific, and unlikely to be suitable for high throughput screening assays. Notable in this regard is neutron activation of select industry relevant metal/metal oxides of different sizes and shapes followed by gamma spectroscopy monitoring, which was used to validate the aforementioned dosimetric platform. Recent publications show that the dosimetric approach used here is reasonably accurate (Cohen et al., 2014a, DeLoid et al., 2014, Cohen et al., 2014b). The dosimetry platform employed in this manuscript has been validated for a number of materials at various time points (Cohen et al., 2014a). The authors are also working to develop more sophisticated multidimensional mathematical models for calculating particle transport *in vitro*, also accounting for dynamic changes to agglomerate properties over time that can influence particle delivery to cells (dissolution, slight shifts in agglomerate diameter and density distributions, etc.) using a variety of metal oxides of different sizes and shapes (Cohen et al., 2014a).

The deposited dose rate is ENM and media dependent (Figure 4). For carbon based ENMs, the deposited doses varied from 20% to 50% of the administered doses at 24h, whereas for the metal/metal oxides with larger effective densities of their formed agglomerates, the deposited doses were much closer to the administered doses for the 24 hour time point. Discrepancies between the administered and delivered doses were more striking during the first few hours. The delivered dose of all ENM was <30% during the first 6 h. This can be explained on the basis of effective density of agglomerates in solution. As indicated in Table 3, it takes nearly 3–4 times more time to deposit 90% of the administered doses for carbon based ENMs, in comparison to metal/metal oxide nanoparticles. These observations highlight the importance of estimation of deposited dose for all ENMs for cellular toxicity evaluations. From the C-based ENMs included in this study, N110 and Printex-90 are often used as *in vitro* comparative materials due to their prevalence in the atmospheric environment. The implications of our findings related to delivered doses for these C-based materials are that a large body of *in vitro* data containing these and other similar materials may need to be reanalyzed to take into consideration dosimetry.

It has to be stated, that the DLS reported Z-Average Hydrodynamic diameter $d_{(h, z\text{-}ave)}$, is a light scattering intensity-weighted average. However, particle fate and transport should ideally be calculated based on a volume-weighted average since density is also based on a hydrodynamic agglomerate volume. To investigate this further we back calculated the volume weighted size distributions for all materials, assuming spherical agglomerates, and compared the volume-weighted averages with the intensity-weighted averages (data not shown). We observed close agreement between the two values for all materials except for Printex-90 particles, which exhibited an intensity weighted diameter 30% larger than its volume weighted average diameter. Using the volume weighted average diameter as an input to the fate and transport model, the estimated deposited dose was within 2% of that calculated based on the intensity weighted average diameter, suggesting for this material the DLS reported hydrodynamic diameter is appropriate for dosimetry calculations.

Implications of dosimetry on hazard ranking in-vitro

One important inquiry in any toxicological evaluation is elucidating the strength of association in the dose-response relationship. *In vitro*, this relationship should be adjusted to take into account the effective dose to cells and this should be done for all materials involved in the study including the positive and negative control ENMs. Because all *in vitro* nanotoxicology is to some extent comparative in nature due to the use of controls and reference materials, one issue of particular interest is the extent to which the strength of association and rank order of toxicity of such materials changes when dose-response data are corrected for the delivered dose. Furthermore, accurate delivered to cell dose estimates are important in order to match *in-vivo* or tissue doses with *in-vitro* ones for validation purposes. We investigate this question with two common endpoints in this study: cell viability and production of IL-8, a pro-inflammatory cytokine in THP-1 cells.

As illustrated in Figure 6 and summarized in Table 5, the slope of dose-response changed considerably when the delivered doses to cells are taken into consideration for some ENMs but not for others. This is expected primarily because some ENMs settle faster than others, as indicated above. The slope of a dose-response relationship has been proposed as a better measure of association for comparative purposes (Rushton et al., 2010). The ratios of slopes based on delivered and administered doses varied from 1.02 for TiO_2 P25 (i.e. essentially the same relationship) to 5.55 for SWCNH-ox (i.e. 555% difference). IC25, the mass dose at which 75% of cells were alive, were determined from individual slopes of regression lines. IC50 could not be reached experimentally for ENMs over the reasonable dose range of 1–50 μg/mL. At higher doses, we have noted significant interactions between ENM and measured endpoints, including cytokine analysis, and other dyes. Based on the slope values of cell viability in THP-1 cells as a function of delivered dose, the ascending rank order (from low to high) of this set of ENM is: TiO_2 P25 < CeO_2 < nAg < MnOx PALAS < Ni-Inco < Printex-90 < N110 < SWCNH-ox. SWCHN-ox had the maximum negative slope followed by N110 and Printex-90 in the carbon based series. In Metal/Metal oxide series Ni-Inco had maximum negative slope followed by MnOx PALAS and nAg. TiO_2 P25 and CeO_2 were the least cytotoxic ENM. The slopes for Carbon based ENMs for deposited masses were significantly different than for administered masses. The same ascending rank order based on the administered dose would be much different: TiO_2 P25 <CeO_2 < nAg < N110 < MnOx PALAS < Printex-90 < SWCNH-ox < Ni-Inco. Direct comparison of cell viability slopes with *in vivo* lung inflammation (Figure 8) for five ENM (TiO_2 P25, CeO_2, nAg, and Printex-90) matches much better ranking based on the delivered dose than the administered dose. Implications of such toxicological analysis in terms of relative ranking are clear.

Comparisons based on other molecular endpoints, such as IL-8 production, are less straightforward to analyze and interpret. Again, for comparison purposes we determined the slope of IL-8 production as a function of administered and delivered doses. Slopes of dose-response would be better suited for subsequent quantitative analysis and comparison between ENM (Table 5). Inflammogenic potential of this set of ENMs, as measured by/reflected in IL-8 production, varied considerably between each ENM. The ascending rank order based on the delivered dose was considerably different as observed from that of administered dose: TiO_2 P25 < CeO_2 < Ni-Inco < MnOx PALAS < nAg < Printex-90 <

N110 < SWCNH-ox. The analysis here focused only on the 24 h time point. Similar calculations done for the 6h time point, paint a similar qualitative picture on dose-response relationships, except that discrepancies in the delivered doses between materials are smaller, as one would expect from deposition data in Figure 4. It has to be acknowledged, that the ranking shown here for PMA matured THP-cells might differ for other cell lines, as final cellular toxicity can be influenced by the different uptake mechanisms and interaction of nanomaterial with cells used in the study. Moreover, the cellular toxicity pathways can vary among cell types (epithelial, mesenchymal etc.) to account for different hazard ranking of ENMs. The methodology presented here though is applicable to other cell types.

In this investigation we used a fixed range of administered doses, 1–50μg/mL. It is important to know how *in vitro* doses-both administered and delivered-compare to the real-world doses. This issue can and should be addressed quantitatively using for example the approach adopted by the authors in two recent studies (Khatri et al., 2013, Demokritou et al., 2013). Authors used the Multiple Path Particle Deposition (MPPD2) model (Anjilvel and Asgharian, 1995) to derive the lung deposited surface dose [$\mu g/m^2$] of nanoparticles using realistic aerosol size distributions and converted these deposited doses to equivalent *in vitro* mass doses. Sensitivity analysis can be further employed to adjust dose ranges accordingly by varying exposure and physiological parameters employed in these models. The range of doses employed here is reasonable for the intended purposes. However, it is also possible that reverse calculations may be employed in future studies to match tested ENM not on their administered, but rather on their delivered doses.

Conclusions

The methodology tested and presented here is suitable for other low aspect ratio ENM, for which the recently developed at Harvard HDDP dosimetry approach is reasonably accurate. Well-dispersed, stable and reproducible suspensions were obtained for all ENMs. The Z-average hydrodynamic diameter ($d_{(h,\ z\text{-}ave)}$, 180–300 nm) and polydispersity index PdI (0.2–0.4) were fairly stable over 24 h, with minor exceptions. Surface charge in water varied considerably between ENMs. These differences disappeared as protein-coated ENM acquired the surface charge of the dispersion medium. Delivered doses were found to be ENM dependent. Over five-fold differences were found in the deposited to cell dose fraction constants for this set of ENMs. For the specific endpoints assessed in this study, the slope of dose-response relationship for cell viability and IL-8 production changed considerably for some ENMs but not for all of them, when delivered dose was taken into consideration. This slope change was more pronounced for ENMs with slower settling rates based on effective density and size of formed agglomerates in-vitro. The ratio of slopes for the delivered and administered doses varied between 1.02 and 5.58. The rank order of these ENMs also shifted notably indicating the importance of including dosimetry in in-vitro screening studies. High aspect ratio ENM continue to remain a challenge and further technological and modeling development are needed for adequate dosimetry and *in vitro* dose-response analysis. In the interim, off-line characterization techniques are needed for dispersion characterization, concentration analysis, and determination of the delivered dose to cells for high aspect ratio ENM such as carbon nanotubes, nanofibers, and nanorods.

Supplementary Material

Refer to Web version on PubMed Central for supplementary material.

Acknowledgments

The study was supported by Nanoscale Science and Engineering Centers Program of the National Science Foundation # 0425826 and EEC-0425826 (Supplement), National Science Foundation (grant no. 1235806) and NIH (grant no. P30ES000002). Authors would like to acknowledge Prof. Daniel F. Schmidt, Prof. Peter Gaines from University of Massachusetts Lowell and Prof. Donald K. Milton from University of Maryland, College Park for insightful discussions and feedback on the work. Special thanks go to Prof. Alison Elder of University of Rochester for her generous sharing of a number of nanomaterials used in this study and the associated *in vivo* lung inflammation data.

Abbreviations

DLS	Dynamic light scattering
DSE	Delivered Sonication Energy
DSE_{cr}	Critical Delivered Sonication Energy
$d_{(hz\text{-}ave)}$	Z-Average Hydrodynamic diameter
ENM(s)	Engineered nanomaterial(s)
FBS	Fetal bovine serum
VCM	Volumetric Centrifugation Method
ISDD	The *in-vitro* sedimentation, diffusion and dosimetry model
IL-8	Interleukin -8
Me/MeOx	Metal/Metal oxide
PBS	Phosphate buffer saline
TRPS	Tunable resistive pulse sensing technology

References

AHMAD KHANBEIGI R, KUMAR A, SADOUKI F, LORENZ C, FORBES B, DAILEY LA, COLLINS H. The delivered dose: Applying particokinetics to in vitro investigations of nanoparticle internalization by macrophages. J Control Release. 2012; 162:259–66. [PubMed: 22824784]

ANDERSON W, KOZAK D, COLEMAN VA, JAMTING AK, TRAU M. A comparative study of submicron particle sizing platforms: accuracy, precision and resolution analysis of polydisperse particle size distributions. J Colloid Interface Sci. 2013; 405:322–30. [PubMed: 23759321]

ANJILVEL S, ASGHARIAN B. A multiple-path model of particle deposition in the rat lung. Fundam Appl Toxicol. 1995; 28:41–50. [PubMed: 8566482]

AYRES JG, BORM P, CASSEE FR, CASTRANOVA V, DONALDSON K, GHIO A, HARRISON RM, HIDER R, KELLY F, KOOTER IM, MARANO F, MAYNARD RL, MUDWAY I, NEL A, SIOUTAS C, SMITH S, BAEZA-SQUIBAN A, CHO A, DUGGAN S, FROINES J. Evaluating the Toxicity of Airborne Particulate Matter and Nanoparticles by Measuring Oxidative Stress Potential - A Workshop Report and Consensus Statement. Inhalation Toxicology. 2008; 20:75–99. [PubMed: 18236225]

BAISCH B, CORSON N, WADE-MERCER P, GELEIN R, KENNELL A, OBERDORSTER G, ELDER A. Equivalent titanium dioxide nanoparticle deposition by intratracheal instillation and

whole body inhalation: the effect of dose rate on acute respiratory tract inflammation. Particle and fibre toxicology. 2014; 11:5. [PubMed: 24456852]

BELLO D, HSIEH SF, SCHMIDT D, ROGERS E. Nanomaterials properties vs. biological oxidative damage: Implications for toxicity screening and exposure assessment. Nanotoxicology. 2009; 3:249–261.

BIHARI P, VIPPOLA M, SCHULTES S, PRAETNER M, KHANDOGA AG, REICHEL CA, COESTER C, TUOMI T, REHBERG M, KROMBACH F. Optimized dispersion of nanoparticles for biological in vitro and in vivo studies. Part Fibre Toxicol. 2008; 5:14. [PubMed: 18990217]

BUFORD MC, HAMILTON RF JR, HOLIAN A. A comparison of dispersing media for various engineered carbon nanoparticles. Part Fibre Toxicol. 2007; 4:6. [PubMed: 17655771]

COHEN J, DELOID G, PYRGIOTAKIS G, DEMOKRITOU P. Interactions of engineered nanomaterials in physiological media and implications for in vitro dosimetry. Nanotoxicology. 2013; 7:417–31. [PubMed: 22393878]

COHEN JM, DERK R, WANG L, GODLESKI J, KOBZIK L, BRAIN J, DEMOKRITOU P. Tracking translocation of industrially relevant engineered nanomaterials (ENMs) across alveolar epithelial monolayers in vitro. Nanotoxicology. 2014a; 0:1–10.

COHEN JM, TEEGUARDEN JG, DEMOKRITOU P. An integrated approach for the in vitro dosimetry of engineered nanomaterials. Part Fibre Toxicol. 2014b; 11:20. [PubMed: 24885440]

DELOID G, COHEN JM, DARRAH T, DERK R, ROJANASAKUL L, PYRGIOTAKIS G, WOHLLEBEN W, DEMOKRITOU P. Estimating the effective density of engineered nanomaterials for in vitro dosimetry. Nat Commun. 2014; 5:3514. [PubMed: 24675174]

DEMOKRITOU, P.; DELOID, G.; COHEN, J. US Provisional Patent Application No. 61/661,895. 2012. Novel methods of measuring effective density of nanoparticles in fluids.

DEMOKRITOU P, GASS S, PYRGIOTAKIS G, COHEN JM, GOLDSMITH W, MCKINNEY W, FRAZER D, MA J, SCHWEGLER-BERRY D, BRAIN J, CASTRANOVA V. An in vivo and in vitro toxicological characterisation of realistic nanoscale CeO(2) inhalation exposures. Nanotoxicology. 2013; 7:1338–50. [PubMed: 23061914]

ZHOU EH, CW, PIZZO R, COHEN J, DANG Q, DE BARROS PMF, PARK CY, CHEN C, BRAIN JD, BUTLER JP, RUBERTI JW, FREDBERG JJ, DEMOKRITOU P. Assessing the impact of engineered nanoparticles on wound healing using a novel in-vitro bioassay. Nanomedicine. 201410.2217/nnm.14.40

ELDER A, GELEIN R, FINKELSTEIN JN, DRISCOLL KE, HARKEMA J, OBERDORSTER G. Effects of subchronically inhaled carbon black in three species. I. Retention kinetics, lung inflammation, and histopathology. Toxicol Sci. 2005; 88:614–29. [PubMed: 16177241]

HINDERLITER PM, MINARD KR, ORR G, CHRISLER WB, THRALL BD, POUNDS JG, TEEGUARDEN JG. ISDD: A computational model of particle sedimentation, diffusion and target cell dosimetry for in vitro toxicity studies. Part Fibre Toxicol. 2010; 7:36. [PubMed: 21118529]

HSIEH SF, BELLO D, SCHMIDT DF, PAL AK, STELLA A, ISAACS JA, ROGERS EJ. Mapping the biological oxidative damage of engineered nanomaterials. Small. 2013; 9:1853–65. [PubMed: 23423873]

JAN E, BYRNE SJ, CUDDIHY M, DAVIES AM, VOLKOV Y, GUN'KO YK, KOTOV NA. High-content screening as a universal tool for fingerprinting of cytotoxicity of nanoparticles. ACS nano. 2008; 2:928–38. [PubMed: 19206490]

JONES CF, GRAINGER DW. In vitro assessments of nanomaterial toxicity. Adv Drug Deliv Rev. 2009; 61:438–56. [PubMed: 19383522]

KELLER AA, WANG H, ZHOU D, LENIHAN HS, CHERR G, CARDINALE BJ, MILLER R, JI Z. Stability and aggregation of metal oxide nanoparticles in natural aqueous matrices. Environ Sci Technol. 2010; 44:1962–7. [PubMed: 20151631]

KHATRI M, BELLO D, PAL AK, COHEN JM, WOSKIE S, GASSERT T, LAN J, GU AZ, DEMOKRITOU P, GAINES P. Evaluation of cytotoxic, genotoxic and inflammatory responses of nanoparticles from photocopiers in three human cell lines. Part Fibre Toxicol. 2013; 10:42. [PubMed: 23968360]

KREWSKI D, ACOSTA D JR, ANDERSEN M, ANDERSON H, BAILAR JC 3RD, BOEKELHEIDE K, BRENT R, CHARNLEY G, CHEUNG VG, GREEN S JR, KELSEY KT, KERKVLIET NI, LI

AA, MCCRAY L, MEYER O, PATTERSON RD, PENNIE W, SCALA RA, SOLOMON GM, STEPHENS M, YAGER J, ZEISE L. Toxicity testing in the 21st century: a vision and a strategy. J Toxicol Environ Health B Crit Rev. 2010; 13:51–138. [PubMed: 20574894]

LIMBACH LK, LI Y, GRASS RN, BRUNNER TJ, HINTERMANN MA, MULLER M, GUNTHER D, STARK WJ. Oxide Nanoparticle Uptake in Human Lung Fibroblasts: Effects of Particle Size, Agglomeration, and Diffusion at Low Concentrations. Environmental science & technology. 2005; 39:9370–9376. [PubMed: 16382966]

LUYTS K, NAPIERSKA D, NEMERY B, HOET PHM. How physico-chemical characteristics of nanoparticles cause their toxicity: complex and unresolved interrelations. Environmental Science: Processes & Impacts. 2013; 15:23–38. [PubMed: 24592425]

MA JY, ZHAO H, MERCER RR, BARGER M, RAO M, MEIGHAN T, SCHWEGLER-BERRY D, CASTRANOVA V, MA JK. Cerium oxide nanoparticle-induced pulmonary inflammation and alveolar macrophage functional change in rats. Nanotoxicology. 2011; 5:312–325. [PubMed: 20925443]

NEL A, XIA T, MENG H, WANG X, LIN S, JI Z, ZHANG H. Nanomaterial toxicity testing in the 21st century: use of a predictive toxicological approach and high-throughput screening. Acc Chem Res. 2013a; 46:607–21. [PubMed: 22676423]

NEL AE, NASSER E, GODWIN H, AVERY D, BAHADORI T, BERGESON L, BERYT E, BONNER JC, BOVERHOF D, CARTER J, CASTRANOVA V, DESHAZO JR, HUSSAIN SM, KANE AB, KLAESSIG F, KUEMPEL E, LAFRANCONI M, LANDSIEDEL R, MALLOY T, MILLER MB, MORRIS J, MOSS K, OBERDORSTER G, PINKERTON K, PLEUS RC, SHATKIN JA, THOMAS R, TOLAYMAT T, WANG A, WONG J. A multi-stakeholder perspective on the use of alternative test strategies for nanomaterial safety assessment. ACS nano. 2013b; 7:6422–33. [PubMed: 23924032]

POWERS KW, BROWN SC, KRISHNA VB, WASDO SC, MOUDGIL BM, ROBERTS SM. Research strategies for safety evaluation of nanomaterials. Part VI. Characterization of nanoscale particles for toxicological evaluation. Toxicol Sci. 2006; 90:296–303. [PubMed: 16407094]

ROBERTS GS, KOZAK D, ANDERSON W, BROOM MF, VOGEL R, TRAU M. Tunable nano/micropores for particle detection and discrimination: scanning ion occlusion spectroscopy. Small. 2010; 6:2653–8. [PubMed: 20979105]

RUSHTON EK, JIANG J, LEONARD SS, EBERLY S, CASTRANOVA V, BISWAS P, ELDER A, HAN X, GELEIN R, FINKELSTEIN J, OBERDORSTER G. Concept of assessing nanoparticle hazards considering nanoparticle dosemetric and chemical/biological response metrics. J Toxicol Environ Health A. 2010; 73:445–61. [PubMed: 20155585]

SAGER TM, CASTRANOVA V. Surface area of particle administered versus mass in determining the pulmonary toxicity of ultrafine and fine carbon black: comparison to ultrafine titanium dioxide. Part Fibre Toxicol. 2009; 6:15. [PubMed: 19413904]

SAGER TM, PORTER DW, ROBINSON VA, LINDSLEY WG, SCHWEGLER-BERRY DE, CASTRANOVA V. Improved method to disperse nanoparticles forin vitroandin vivoinvestigation of toxicity. Nanotoxicology. 2007; 1:118–129.

SHARMA G, KODALI V, GAFFREY M, WANG W, MINARD KR, KARIN NJ, TEEGUARDEN JG, THRALL BD. Iron oxide nanoparticle agglomeration influences dose rates and modulates oxidative stress-mediated dose-response profiles in vitro. Nanotoxicology. 2014; 8:663–75. [PubMed: 23837572]

SUMMERS HD, REES P, HOLTON MD, BROWN MR, CHAPPELL SC, SMITH PJ, ERRINGTON RJ. Statistical analysis of nanoparticle dosing in a dynamic cellular system. Nat Nanotechnol. 2011; 6:170–4. [PubMed: 21258333]

TEEGUARDEN JG, HINDERLITER PM, ORR G, THRALL BD, POUNDS JG. Particokinetics in vitro: dosimetry considerations for in vitro nanoparticle toxicity assessments. Toxicol Sci. 2007; 95:300–12. [PubMed: 17098817]

THOMAS CR, GEORGE S, HORST AM, JI Z, MILLER RJ, PERALTA-VIDEA JR, XIA T, POKHREL S, MADLER L, GARDEA-TORRESDEY JL, HOLDEN PA, KELLER AA, LENIHAN HS, NEL AE, ZINK JI. Nanomaterials in the environment: from materials to high-throughput screening to organisms. ACS nano. 2011; 5:13–20. [PubMed: 21261306]

VANWINKLE BA, DE MESY BENTLEY KL, MALECKI JM, GUNTER KK, EVANS IM, ELDER A, FINKELSTEIN JN, OBERDÖRSTER G, GUNTER TE. Nanoparticle (NP) uptake by type I alveolar epithelial cells and their oxidant stress response. Nanotoxicology. 2009; 3:307–318. [PubMed: 20563262]

VIPPOLA M, FALCK GC, LINDBERG HK, SUHONEN S, VANHALA E, NORPPA H, SAVOLAINEN K, TOSSAVAINEN A, TUOMI T. Preparation of nanoparticle dispersions for in-vitro toxicity testing. Hum Exp Toxicol. 2009; 28:377–85. [PubMed: 19755449]

WARHEIT DB, BORM PJ, HENNES C, LADEMANN J. Testing strategies to establish the safety of nanomaterials: conclusions of an ECETOC workshop. Inhalation Toxicology. 2007; 19:631–43. [PubMed: 17510836]

WATSON CG, JING, COHEN JOEL, PYRGIOTAKIS GEORGIOS, ENGELWARD BEVIN, DEMOKRITOU PHILIP. A High Throughput Screening Platform for Engineered Nanoparticle Mediated Genotoxicity using CometChip Technology. ACS nano. 2014 In press.

WILLMOTT GR, VOGEL R, YU SS, GROENEWEGEN LG, ROBERTS GS, KOZAK D, ANDERSON W, TRAU M. Use of tunable nanopore blockade rates to investigate colloidal dispersions. J Phys Condens Matter. 2010; 22:454116. [PubMed: 21339603]

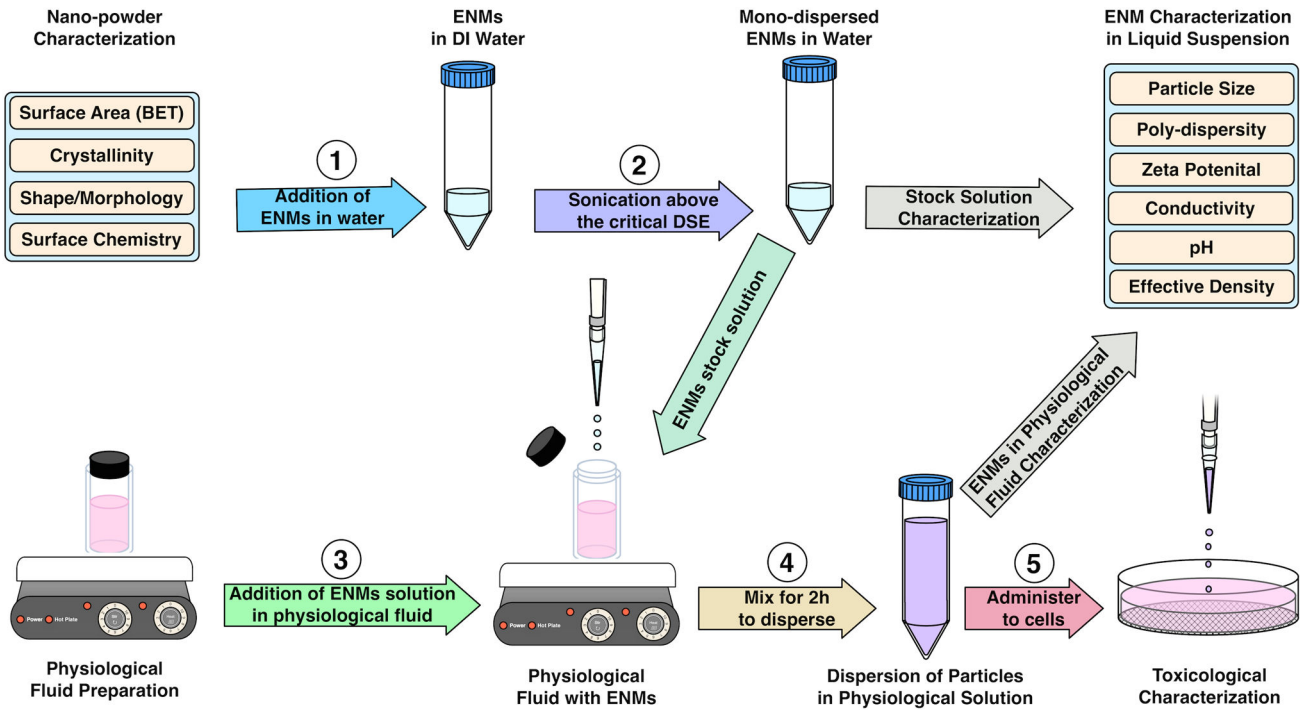

Figure 1.

Schematic illustration of the standardized dispersion protocol for diverse classes of ENMs. Note that in this work two minor modifications were made in the Cohen et al. (2013) protocol: (i) in step 3, FBS (10%) was premixed with the cell culture medium (in this case RPMI) prior to addition of ENM dispersion in water from step 2 instead of only FBS; and (ii) vortexing for 30 sec in step 4 was substituted with a mixing step at 800 rpm for 2 h. As described in the supplemental material, stable dispersions could be achieved only at 10% FBS. In addition, mixing for longer than 2 h did not result in significant gains in dispersion stability.

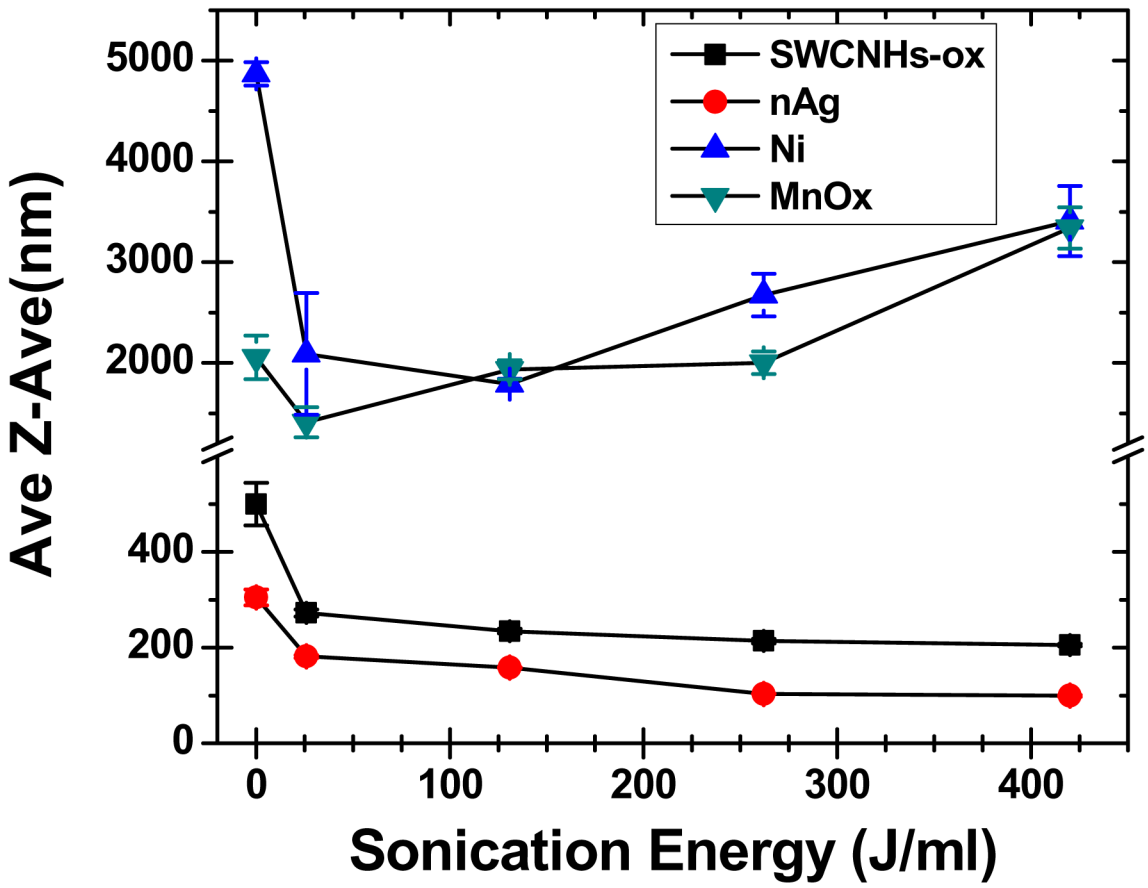

Figure 2.

Relationship between the hydrodynamic diameters ($d_{(h, z\text{-}ave)}$) as a function of delivered sonication energy (DSE) used in determining the critical DSE (DSE_{cr}) for various ENMs. Two distinct patterns were revealed: A) the familiar asymptotic curve as illustrated by SWCNHs-ox and nAg; B) U-shaped, illustrated for Ni Inco and MnOx-PALAS.

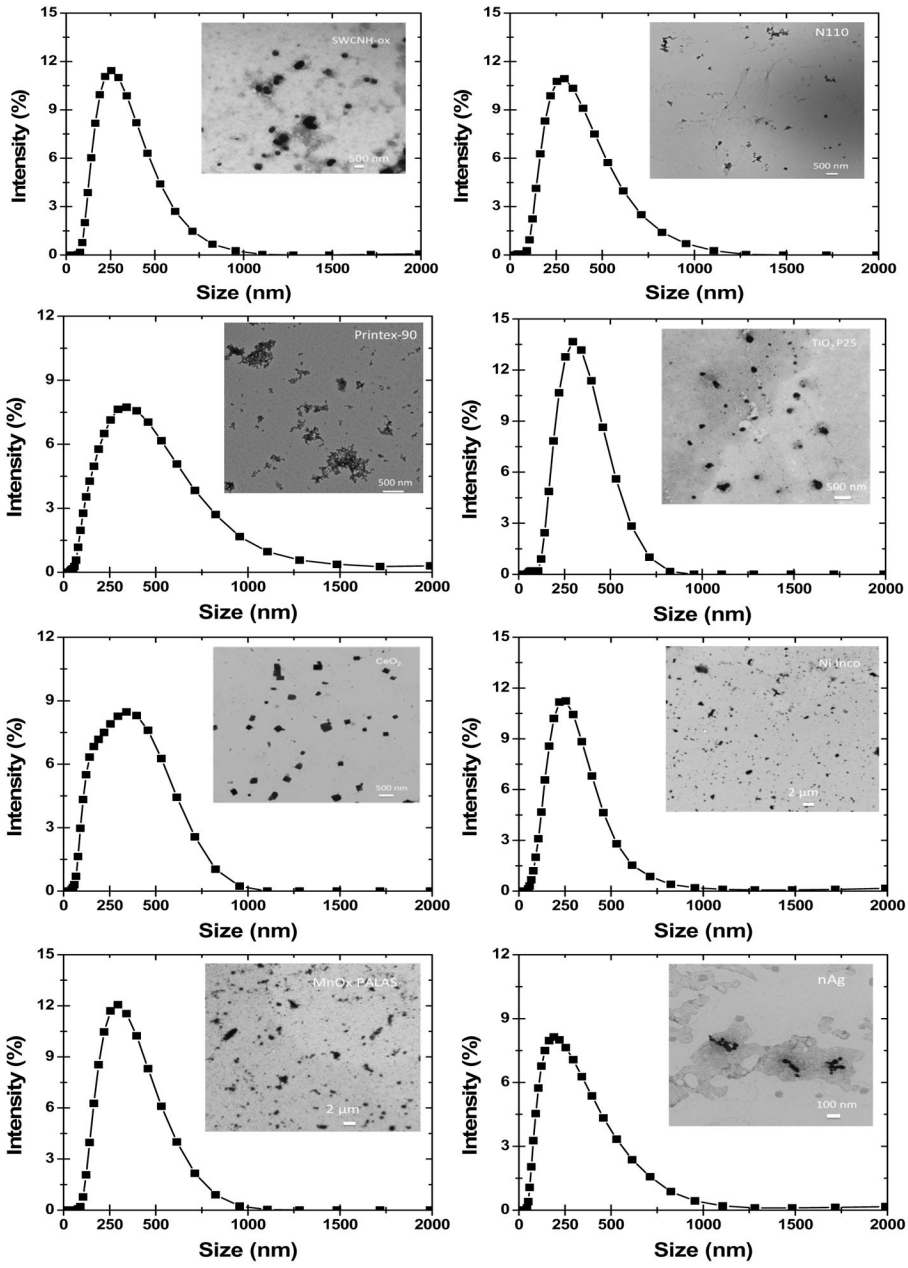

Figure 3.

DLS size distribution and TEM images of ENMs following dispersion protocol in RPMI +10% FBS. All ENMs were diluted in DI water at 50µg/mL concentration from the initial 0.5mg/mL stock suspension in RPMI+10% FBS. Reproduced in parts with permission from Pal et al. *ACS Nano*, **2014**, *8* (9), pp 9003–9015.

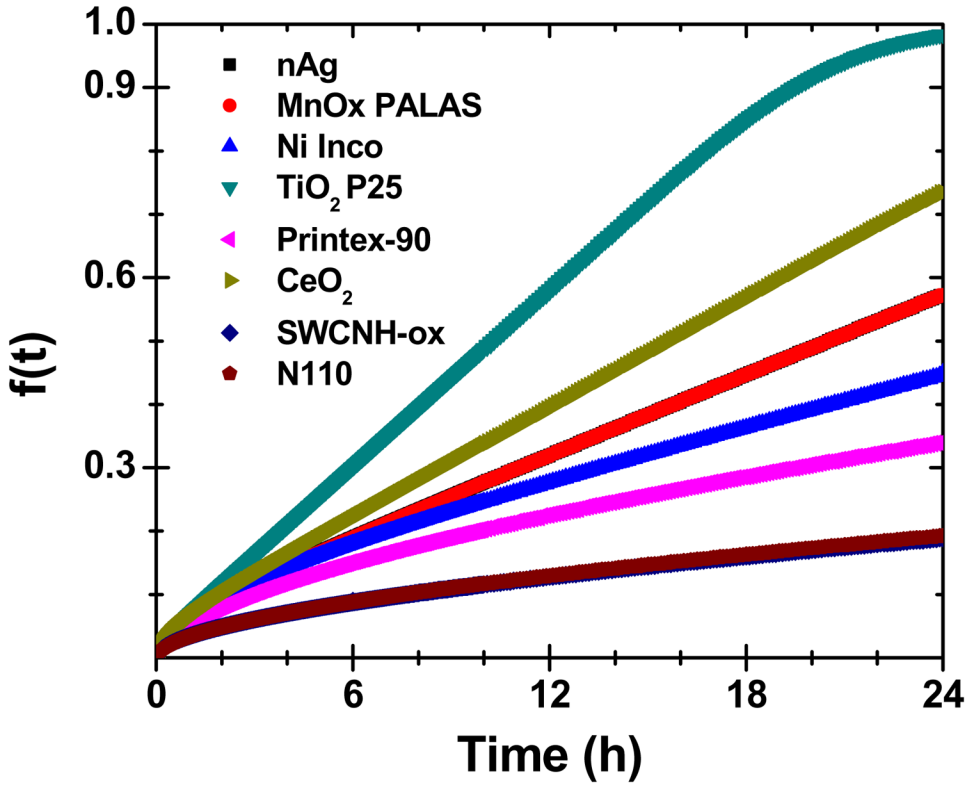

Figure 4.

VCM-ISDD model based calculations for NM delivered dose for different ENM formulations in RPMI+10% FBS medium. Reproduced in parts with permission from Pal et al. *ACS Nano*, **2014**, *8* (9), pp 9003–9015.

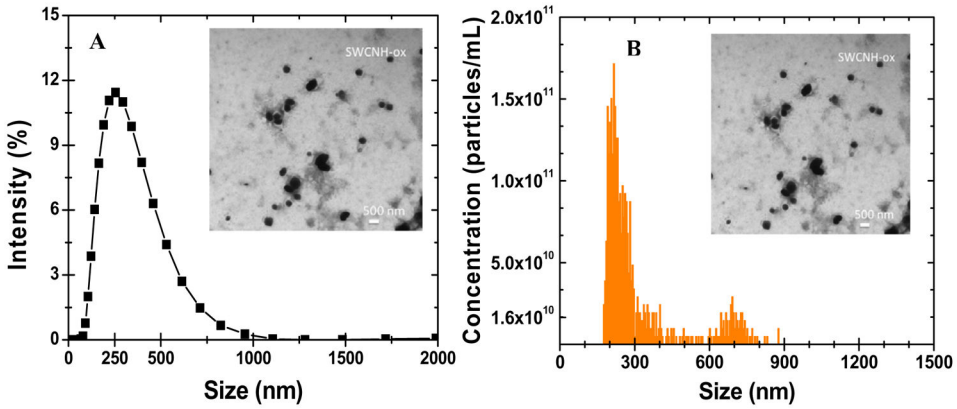

Figure 5.

Representative comparison of DLS and TRPS, dispersion characterization techniques. (a) DLS and TRPS size distributions for SWCNH-ox and (b) particle concentration (particles/ml) as determined by TRPS.

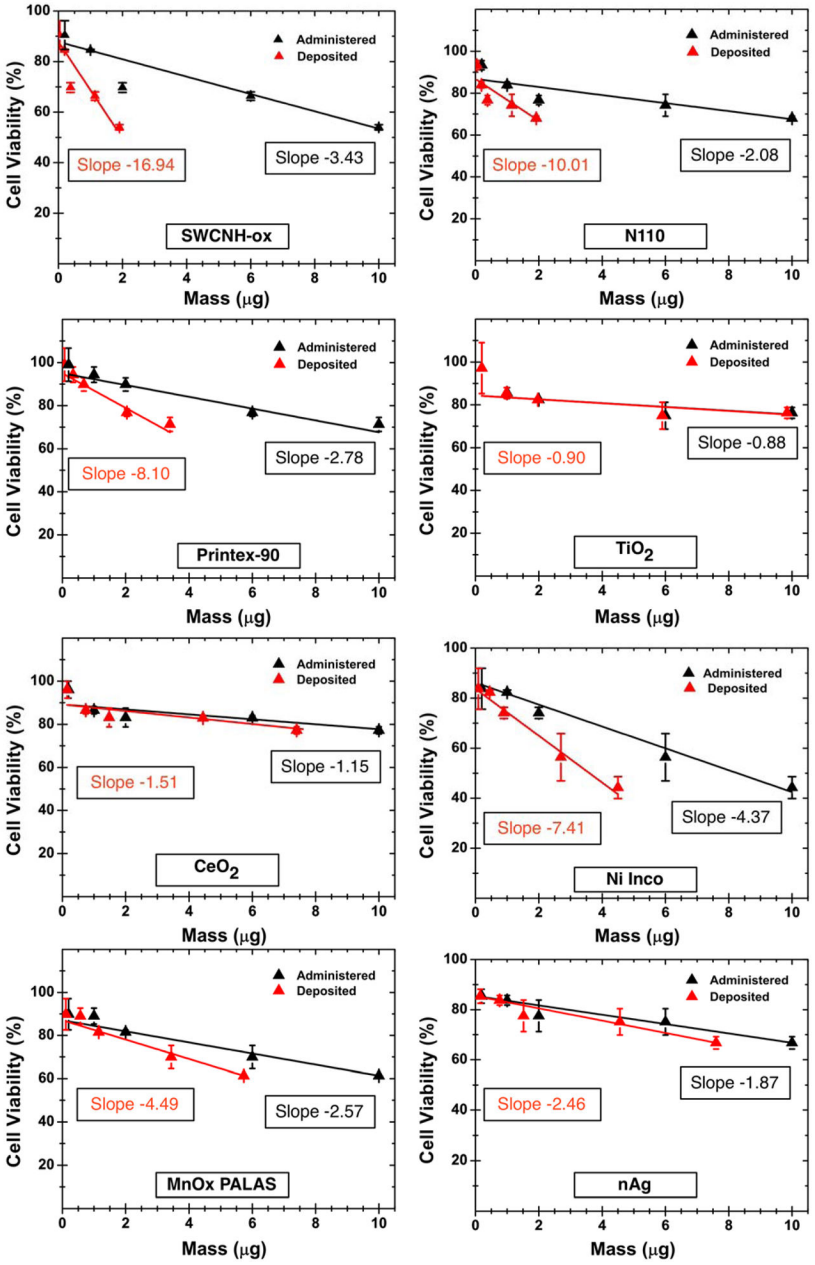

Figure 6.

MTT cell viability assay toxicity results as a function of administered and deposited dose for all ENMs dispersed in RPMI+10% FBS at 24h. Fitted lines for most ENM had an R^2 of 0.9 or better; for N110 (R^2 =0.8), and CeO_2 and TiO2 (R^2 ~0.65). The delivered dose estimates were derived from the VCM-ISDD model calculations with effective density measurements (Hinderliter et al 2010; Cohen et al 2014) reported in table 3. Reproduced in parts with permission from Pal et al. ACS Nano, 2014, 8 (9), pp 9003–9015.

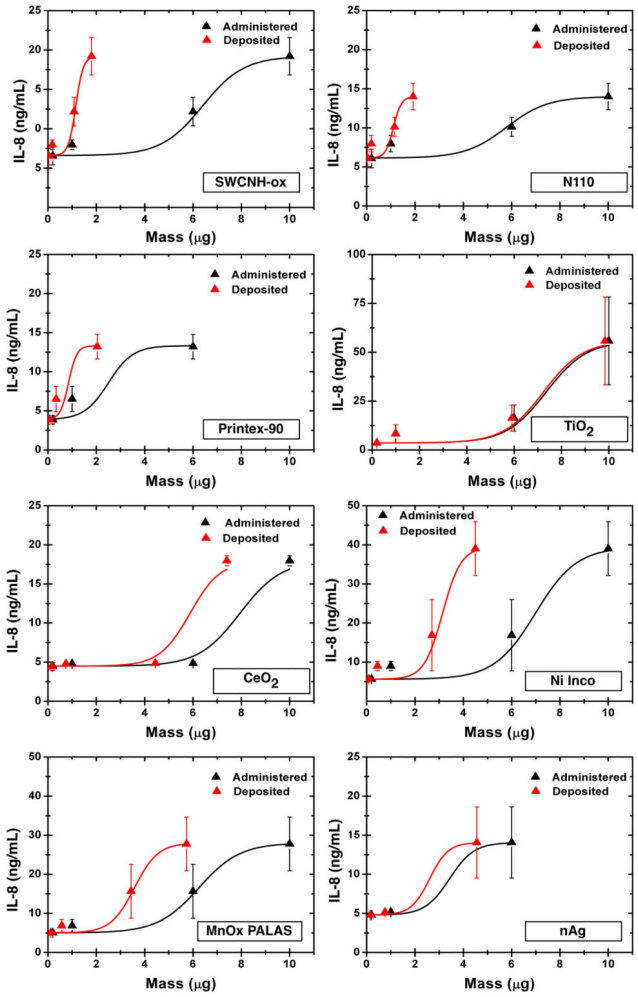

Figure 7.

Dose-response relationship for pro-inflammatory cytokine IL-8 as function of administered and deposited dose over the 1–50μg/mL range. The R^2 of fitted lines was >0.95 for all curves. Slopes used in Table 5 were determined from the Origin software. For Printex-90 and nAg, the IL-8 concentrations at the highest 50 μg/mL dose were above the upper detection limit of the instrument. As reported in the literature, it is possible that the high production rate and much higher variability in IL-8 concentrations may be a result of competing factors: either interaction of ENM with IL-8 and/or due to high ENM cell toxicity. The delivered dose estimates were derived from the VCM-ISDD model calculations with effective density measurements (Hinderliter et al 2010; Cohen et al 2014) reported in table 3.

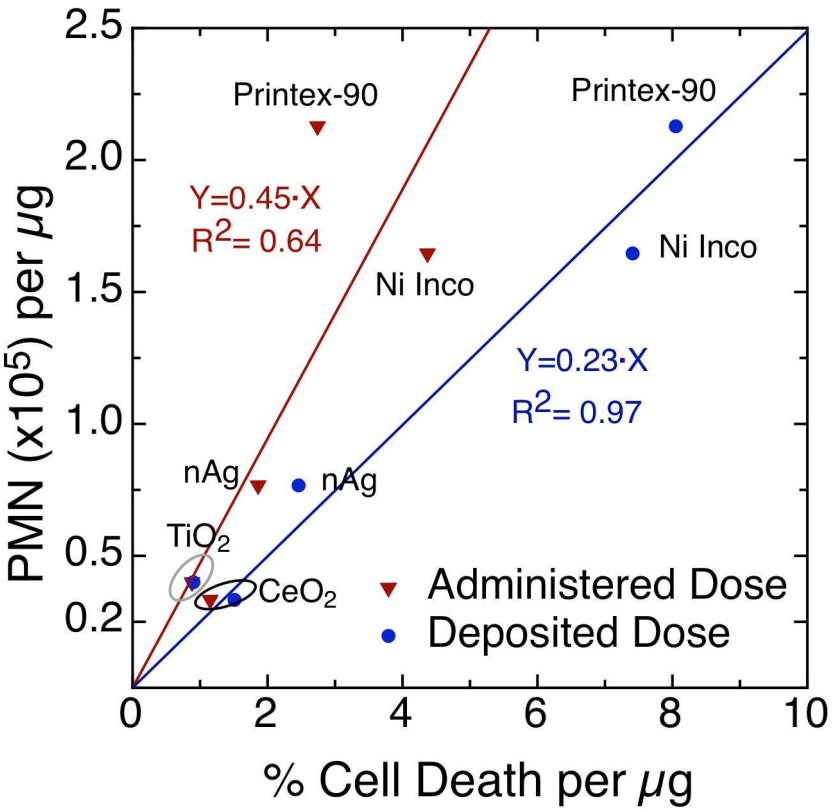

Figure 8.

Comparison of *in vitro* cell death slopes to *in vivo* lung inflammation (PMN/μg) for five test materials. Much stronger association with PMN is observed for deposited dose slopes (R^2=0.97) as compared to administered dose (R^2=0.64), highlighting the importance of considering delivered dose to cells in in vitro nanotoxicology.

Table 1

Summary description of the materials tested in this study.

Sample	Label	Description	Source [Reference]	Primary particle size from vendor	SSA (m^2g^{-1})	ρ (g/cm^3)
1	SWCNHs-ox	Single Wall Carbon Nanohorns, H_2O_2 oxidized	Donated by NEC Co., Japan [Bello, 2009; Hsieh, 2013]	OD = 1–2 nm; Aggl. = 50–100 nm	1154	1.25
2	N110	Carbon black N110	Cabot Corp., Billerica MA, USA [Bello, 2009; Hsieh, 2013]	15 nm	111	1.25
3	Printex-90	Carbon black	Degussa [Elder, 2005; Sager, 2009]	14 nm	236	1.85
4	TiO_2 P25	Anatase/Rutile/amorphous ~75/20/5%	Evonic/Degussa; UC Center for Environmental Implications of Nanotechnology [Keller, 2010; VanWinkle, 2009]	25 nm	63	4.25
5	CeO_2	Cerium oxide	UC Center for Environmental Implications of Nanotechnology [Keller, 2010]	7–25 nm	87	7.65
6	Ni Inco [a]	Nickel nanoparticles	Inco specialty powders; Donated from Prof. A. Elder, U Rochester	60 ±10 nm	91	8.19
7	MnOx PALAS [b]	Manganese oxide	Donated from Prof. A. Elder, U Rochester [VanWinkle, 2009]	40 nm	58	5.03
8	nAg	Nano-silver	Donated from Prof. A. Elder, U Rochester [VanWinkle, 2009; Rushton 2010]	35 nm	18	10.50

SSA, Specific surface area; ρ, Material density. The SSA values in the table represent our own BET measurements, which may differ slightly from published values. Reproduced in parts with permission from Pal et al. ACS Nano, 2014, 8 (9), pp 9003–9015.

[a] Ni Inco (Rochester, NY), high surface area Ni powder for catalytic applications, produced via carbonyl-based chemical vapor deposition technology and partially surface oxidized. ICP-MS analysis yielded 69% Ni, 0.5% Mn, <0.01% Fe, and 1–20 ppm of other elements. Water-soluble Ni was 4%. B.

[b] MnOx contained 61% Mn, 0.41% Ni, and 700 ppm Cu, 260 ppm Fe, 100 ppm Ag, and 30 ppm Mo. Water-soluble Mn accounted for 14.3%.

Table 2

Characterization ($d_{(h, z\text{-}ave)}$, PdI and zeta) of ENMs in DI water at DSE and after constant mixing of ENM suspension in RPMI+10% FBS for 24h. Afterwards stability of ENMs in RPMI+10 % FBS was determined after 6h and 24h respectively. Reproduced in parts with permission from Pal et al. *ACS Nano*, **2014**, *8* (9), pp 9003–9015.

Material Label	In DI water				After 2hr mixing in RPMI+10%FBS			Dispersion stability after 6 h			Dispersion stability after 24 h		
	DSE_{cr} *(J/ml)*	$d_{(h, z\text{-}ave)}$ *(nm)*	*PdI*	*Zeta ζ (mV)*	$d_{(h, z\text{-}ave)}$ (nm)	*PdI*	*Zeta ζ (mV)*	$d_{(h, z\text{-}ave)}$ (nm)	*PdI*	*Zeta ζ (mV)*	$d_{(h, z\text{-}ave)}$ (nm)	*PdI*	*Zeta ζ (mV)*
SWCNHs-ox	161	213.5±5.1	0.21	−29.7±0.2	275.30±2.6	0.27	−11.17±0.3	260.47±1.9	0.24	−12.9±1.2	275.4±2.4	0.27	−13.8±1.2
N110	262	181.7±3.5	0.20	−20.9±2.2	261.07±2.0	0.23	−11.93±0.6	278.63±6.3	0.36	−11.1±0.9	270.3±4.0	0.37	−12.5±0.8
Printex-90	262	187.7±2.6	0.40	17.4±2.1	287.87±10.1	0.42	−12.00±0.3	258.67±3.4	0.41	−12.2±0.5	252.1±6.3	0.36	−12.9±1.9
TiO_2 P25	161	336.0±9.0	0.39	19.5± 1.5	350.60±3.1	0.32	−11.90±1.2	280.80±3.9	0.29	−12.1±1.1	281.8±2.9	0.33	−12.7±1.2
CeO_2	262	127.0±16.4	0.35	34.5±3.1	286.47±25.5	0.31	−12.57±1.9	214.63±6.3	0.56	−15.1±3.8	223.6±7.9	0.50	−14.6±0.7
Ni Inco	262	1791.3 ± 51.7	0.61	16.8±2.8	215.00±3.8	0.39	−11.37±0.2	303.57±30.2	0.74	−10.0±1.8	280.3±16.0	0.92	−12.3±1.4
MnOx PALAS	161	1489.5 ± 44.5	0.39	7.5±2.4	274.80±4.7	0.15	−12.60±0.1	308.87±1.1	0.44	−12.6±0.7	320.2±5.3	0.47	−11.4±0.9
nAg	262	103.5±0.5	0.47	−30.7±2.7	172.37±4.6	0.39	−11.02±1.6	171.90±3.8	0.41	−11.0±1.0	177.8±1.3	0.39	−12.6±1.4

Table 3

Mass, surface area and particle concentration as cellular dose metric, based on administered and deposited doses for all ENMs dispersed in RPMI+10% FBS at a mass concentration of 50μg/mL following 24h exposure. The dose estimates derived from the ISDD model calculations with effective density measurements (Hinderliter et al 2010; Cohen et al 2012) based on delivered ENM mass dose to cells over time. Reproduced in parts with permission from Pal et al. ACS Nano, 2014, 8 (9), pp 9003–9015.

Nanomaterial Label	Effective density ρ_e (g/cm^3)	Deposition fraction constant α (h^{-1})	t90 (h)	Administered dose		Deposited dose		
				Mass (μg)	SA (cm^2)	Mass (μg)	SA (cm^2)	Particles /cm^2
SWCNHs-ox	1.25	0.010	227.34	10	11.54	1.88	2.17	1.97E+08
N110	1.04	0.010	224.11	10	1.11	1.92	0.21	1.59E+08
Printex-90	1.24	0.020	117.50	10	2.36	3.4	0.80	7.76E+08
TiO_2 P25	1.31	0.082	27.99	10	2.74	9.84	2.70	3.76E+08
CeO_2	1.69	0.046	50.23	10	0.87	7.35	0.64	6.75E+08
Ni Inco	1.78	0.026	88.00	10	0.91	4.46	0.41	5.18E+08
MnOx PALAS	1.52	0.033	68.91	10	0.58	5.73	0.33	5.94E+08
nAg	2.30	0.050	46.37	10	0.18	7.6	0.14	1.38E+09

SA: Surface area

Note: Surface area and particle number concentration dose metrics are based on ISDD model calculations. RID functions can be calculated by inserting appropriate alpha parameter, hydrodynamic diameter and effective density reported in Table 2 into equations 5, 6 or 7 for delivered mass, surface area, and particle number after a given exposure duration.

Table 4

Comparative summary of DLS and TRPS size measurements for tested ENM. Reproduced in parts with permission from Pal et al. ACS Nano, 2014, 8 (9), pp 9003–9015.

ENM Type	Dynamic Light Scattering (DLS)		Tunable Resistive Pulse Sensing (TRPS)			DLS/TRPS Ratio of mean peak sizes
	Mean Size (nm)	PdI	Mean, Small Peak (nm)	Mean, Large Peak (nm)	Large peak, % of total number	
SWCNH-ox	261.4±3.0	0.23	248.9	660.0	0.156	1.05
N110	282.97±3.2	0.27	202.4	-	-	1.39
Printex-90	270.37±8.2	0.37	263.7	1067.8	0.029	1.02
TiO_2 P25	301.00±8.7	0.29	305.5	1042.6	0.013	0.98
CeO_2	265.45±1.9	0.31	267.7	1065.8	0.014	0.99
Ni Inco	233.90±6.9	0.40	267.9	1135.8	0.010	0.87
MnOx PALAS	264.33±0.2	0.23	258.6	1077.7	0.010	1.02
nAg	183.33±6.0	0.34	285.7	1054.8	0.010	0.64

Table 5

Summary of select cell toxicity data for all ENMs dispersed in RPMI+10% FBS for 24h incubation. Slopes were determined for calculating IC25, the mass dose at which 75% of cells were alive. IC50 could not be reached experimentally. The ascending rank order of this set of ENM based on the delivered dose slope of cell viability is: TiO_2 P25< CeO_2 < nAg < MnOx PALAS < Ni Inco < Printex-90 < N110 < SWCNH-ox. The order changes slightly, as follows, if ranking is based on the delivered dose slopes of pro-inflammatory marker IL-8: TiO_2 P25 < CeO_2 < Ni Inco < MnOx PALAS < nAg < Printex-90 < N110 < SWCNH-ox. The PMN data for five of the eight test materials were obtained from the published literature as indicated (TiO_2 P25, Printex-90 and CeO_2) or provided by Prof. A. Elder (nAg, Ni Inco) of University of Rochester, USA. No matching PMN data could be found for the remaining three materials, SWCNH-ox, N110 and MnOx PALAS. Reproduced in parts with permission from Pal et al. ACS Nano, 2014, 8 (9), pp 9003–9015.

	Cell Viability (% Live Cells/μg)				IL-8 Cytokine release (ng/μg*mL)		BAL PMN (×10^5/μg)
Nanomaterial Label	**Slope, Admin.**	**Slope, Delivered**	**Slope Ratio, Delivered/Admin.**	**IC25 (Delivered Dose)**	**Slope, Admin**	**Slope, Delivered**	
SWCNH-ox	−3.43	−16.94	**4.94**	0.58	0.51	2.83	-
N110	−2.08	−10.01	**4.81**	1.22	0.51	2.66	-
Printex-90	−2.78	−8.10	**2.91**	2.73	0.86	2.53	2.13 (Sager 2010)
TiO_2 P25	−0.88	−0.90	**1.02**	17.24	0.51	0.52	0.16; 0.4 (Baisch 2014) [a] 0.44 (Sager 2010)
CeO_2	−1.15	−1.51	**1.31**	11.24	0.51	0.67	0.33 (Ma 2011)
Ni Inco	−4.37	−7.41	**1.69**	1.61	0.51	0.70	1.65 (A. Elder)
MnOx PALAS	−2.57	−4.49	**1.75**	4.35	0.51	0.90	-
nAg	−1.87	−2.46	**1.32**	4.21	0.86	1.13	0.77 (A. Elder)

[a] Low dose of 39.24 μg resulted in 6.10 × 10^5 BAL PMNs (0.16); High dose of 163.58 μg resulted in 65.02 × 10^5 BAL PMNs (0.44 PMN/μg). Average PMN calculated from all three TiO_2 P25 doses was used for final analysis.